Large work function reduction by adsorption of a molecule with a negative electron affinity: Pyridine on ZnO$(10\bar{1}0)$

Oliver T. Hofmann,[1, a)] Jan-Christoph Deinert,[1] Yong Xu,[1] Patrick Rinke,[1] Julia Stähler,[1, b)] Martin Wolf,[1] and Matthias Scheffler[1]

Fritz-Haber-Institut der Max-Planck-Gesellschaft, Faradayweg 4-6, 14195 Berlin, Germany

(Dated: 25 September 2013)

Using thermal desorption and photoelectron spectroscopy to study the adsorption of pyridine on ZnO$(10\bar{1}0)$, we find that the work function is significantly reduced from 4.5 eV for the bare ZnO surface to 1.6 eV for one monolayer of adsorbed pyridine. Further insight into the interface morphology and binding mechanism is obtained using density functional theory. Although semilocal density functional theory provides unsatisfactory total work functions, excellent agreement of the work function *changes* is achieved for all coverages. In a closed monolayer, pyridine is found to bind to every second surface Zn atom. The strong polarity of the Zn-pyridine bond and the molecular dipole moment act cooperatively, leading to the observed strong work function reduction. Based on simple alignment considerations, we illustrate that even larger work function modifications should be achievable using molecules with negative electron affinity. We expect the application of such molecules to significantly reduce the electron injection barriers at ZnO/organic heterostructures.

I. INTRODUCTION

Controlling the work function (Φ) of semiconductor crystals by adsorbing tailor-made organic molecules on the surface is of potential interest for a large variety of fields and applications. These include established industrial products such as varistors,[1–3] where the work function determines the varistor voltage, and more recently inorganic/organic hybrid devices[4–7] like organic photovoltaic cells and light-emitting devices. There, the position of the molecular frontier orbitals relative to the Fermi energy determines charge injection and extraction barriers[7–12] and thus important properties like, e.g., the driving voltage in light-emitting devices. It is well established that the substrate work function can be tuned by creating a periodic array of dipoles at the surface.[13] Such a sheet can be obtained, e.g., by adsorbing self-assembled monolayers (SAMs).[14–25] The origin of the implied work function change, $\Delta\Phi$, is of electrostatic nature and is given by the solution of the Helmholtz-equation

$$\Delta\Phi = \frac{-q_e}{\epsilon_0}\frac{\mu}{A} \tag{1}$$

where q_e is the elementary charge, ϵ_0 the vacuum dielectric constant, and μ/A the surface dipole density. μ consists of various different contributions, including the intrinsic molecular dipole moment, depolarization from the surrounding medium, bond and image dipole formation as well as potential band-bending.

Amines are particularly well suited to achieve large work function reductions, since they can easily form strong bonds to a variety of different surfaces while carrying a significant intrinsic dipole of their own. For aliphatic amines, work function reductions between 1 and 2 eV have been found on ZnO$(10\bar{1}0)$ and several other surfaces.[26–30] For aromatic amines, such as pyridine and its derivates, work function reductions larger than 1 eV are commonly reported.[24,31–37] On Pt and Au, the adsorption-induced work function change could even yield -2.5 eV or more.[24,31,37] Pyridine is also commonly used in organic layers as "docking group",[24,38] and the application of pyridine-containing polymers has been demonstrated to improve the stability and electron transport properties of organic electronic devices, while simultaneously enabling the use of high Φ materials as electrodes.[38] Optoelectronic organic devices, in particular photovoltaic cells and light-emitting devices, require at least one optically transparent electrode. This cannot be achieved with metal substrates, which by definition have no band gap. There is, therefore, a renewed interest in surface modifications of conductive transparent oxides, in particular ZnO, which is non-toxic, cheap, abundant, and optically transparent up to energies of 3.3 eV.[39] Previous studies on polar and non-polar ZnO surfaces indicate that pyridine reproducibly forms highly oriented structures.[40,41] In the present work, we report that a proper preparation of pyridine/ZnO$(10\bar{1}0)$ interfaces yields work function reductions as large as 2.9 eV. The adsorption geometry, binding mechanism and interface dipoles are studied for a variety of pyridine coverages using photoelectron spectroscopy, thermal desorption spectroscopy and density functional theory augmented with the van-der-Waals scheme of Tkatchenko and Scheffler (vdW-TS).[42] The application of standard density functionals is often criticized,[43,44] mostly because of the erroneous position of Kohn-Sham levels due to electron self-interaction[45,46] and the failure to account for the orbital renormalization at the interface.[47–50] Applying hybrid density functionals with an adjustable fraction

[a)] Electronic mail: hofmann@fhi-berlin.mpg.de
[b)] Electronic mail: staehler@fhi-berlin.mpg.de

of exact exchange, we show that despite the sensitivity of the Kohn-Sham orbitals to the applied methodology, the adsorption-induced dipole is insensitive to the fraction of exact exchange and already well described with common semilocal functionals. This lends further credibility to our calculations and allows us to formulate a pathway towards systems with even stronger work function reductions.

II. EXPERIMENTAL AND COMPUTATIONAL METHODOLOGY

The ZnO($10\bar{1}0$) surface was prepared by sputtering and annealing cycles and exposed at T=100 K to pyridine vapor (Sigma Aldrich, 99.8%) via a pinholer doser. The quality of the bare ZnO($10\bar{1}0$) surface was confirmed by low-energy electron diffraction (LEED) and photoelectron spectroscopy (PES). Pyridine desorption was monitored by thermal desorption (TD) spectroscopy, where the integral of the spectrum serves as mass equivalent for coverage calibration. PES was performed using the second harmonic of the output of an optical parametric amplifier ($h\nu = 3.76$ eV), driven by a regeneratively amplified femtosecond laster system (100 kHz). The photoelectrons were detected using a hemispherical electron analyzer. The work function was determined by the low energy cut-off in the PE spectra, originating from electrons that barely overcome the vacuum barrier E_{vac}. Depending on the magnitude of the work function (smaller or larger than the photon energy), one- or two-photon photoemission (1PPE or 2PPE, respectively) was used to emit one electron. (Figure 1, right inset). Electron energies were referenced to the Fermi energy E_F of the tantalum sample holder which was in electrical contact to the sample and held at a bias voltage of -5 V with respect to the analyzer.

All calculations were performed using the Fritz Haber Institute *ab initio molecular simulations* (FHI-aims) code,[51] employing the Perdew-Burke-Ernzerhof (PBE) generalized gradient functional[52] and the Heyd-Scuseria-Ernzerhof hybrid functional (HSE).[53] The long-range part of van-der-Waals forces, which are not accounted for in standard semilocal or hybrid functionals, were included by the vdW-TS scheme.[42] For ZnO, the necessary parameters were calculated using the approach described for atoms in solids,[54] yielding $C_6 = 46.0183$, $\alpha = 13.7743$, $r_0 = 2.818$ for Zn and $C_6 = 4.45343$, $\alpha = 4.28501$, $r_0 = 2.953$ for O. "Tight" defaults were used for grids and basis sets. The ZnO substrate was modeled by 8 ZnO layers in the periodic slab approach with a 30 Å vacuum separation and a dipole correction between the periodic images. We optimized all geometries in PBE+vdW by relaxing the atomic position of the molecule and the top 4 ZnO layers until the remaining forces were smaller than 10^{-3} eV/Å, while the bottom 4 layers were fixed to their bulk positions.

The ZnO sample used in this work was intrinsically n-type doped, with a Fermi energy of approx. 200 meV below the conduction band onset. The atomistic origin of n-type conductivity in experimental ZnO samples is still widely debated.[55] In the present work we assume that the doping of the crystal is homogeneous. This implies that the majority of the dopants are located below the surface and interact only electrostatically (rather than via overlap of their wave function) with the adsorbate. This situation is modeled using the virtual crystal approximation.[56–58] There, the oxygen nuclei with $Z = 8$ are replaced by pseudoatoms with $Z = 8 + \Delta Z$.[57,58] The excess electrons ΔZ go to the bottom of the conduction band. We note that the virtual crystal approximation is most reliable for substitutional dopants. Its validity has been widely tested by Richter et al.[57] We used a doping concentration of 4×10^{16} electrons$/cm^3$ ($10^{-6}e^-$/O atom) and verified explicitly that higher doping concentration up to 4×10^{19} give identical results within 10 meV for both the adsorption energy and the interface dipole. This is in sharp contrast to the behavior observed for electron acceptors on ZnO[59] and attributed to the fact that the adsorption of pyridine does not cause appreciable band bending, as explained below.

III. RESULTS AND DISCUSSION

Figure 1a depicts a TD spectrum of 1.1 monolayers (ML) of pyridine acquired using a heating rate of 8 K/min. The main features of the spectrum - a sharp peak at 140 K and a broad feature at slightly higher temperatures - are reminiscent of previous TD studies of pyridine on polar ZnO(0001) surfaces.[41]At 140 K the sharp peak originates from the desorption of weakly bound molecules adsorbed on top of the first monolayer (corrsponding to the broad TD feature) as discussed in the following. The sample work function is measured during heating using 1PPE and 2PPE as shown in Figure 1b. The left inset depicts three representative spectra for different temperatures. As the energies are referenced to the Fermi level, the low-energy cut-off can be used to directly read out the work function. For pristine ZnO it is is determined as 4.52(5) eV and reduces to 1.66(5) eV after deposition of a full monolayer of pyridine. The corresponding work function change, $\Delta\Phi$ = -2.86(8) eV, is significantly larger than the values reported for the adsorption of pyridine on Cu(111)[60] or the prediction on Au(111).[24] Starting with a multilayer coverage, the minimum of the work function occurs at the same temperature (145 K, panel b) as the desorption of the multilayer peak in panel a. Further increasing the temperature (and thus reducing the coverage), the work function increases steadily due to desorption, clearly indicating that the broad TD signal can be attributed to the desorption of the first monolayer of pyridine. Finally, for low coverages, the work function approaches the value corresponding to the clean ZnO surface.

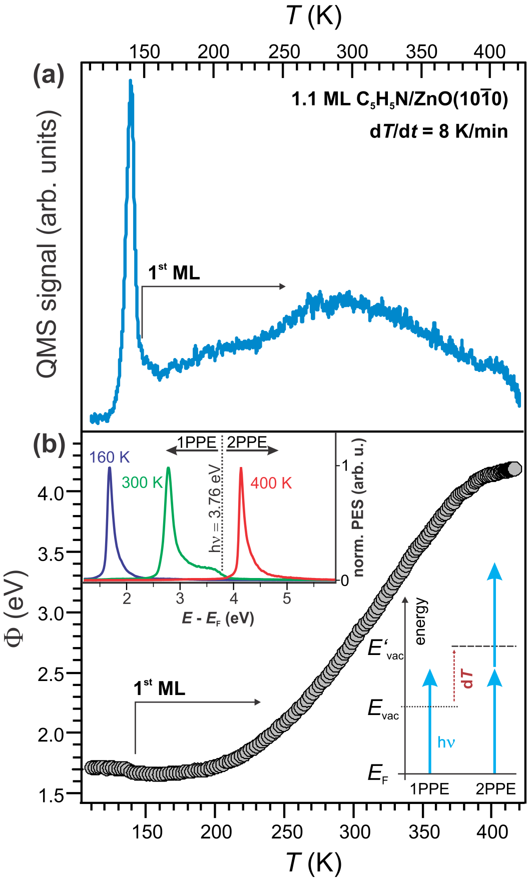

FIG. 1. (a): TD spectrum of 1.1 ML pyridine on ZnO(10$\bar{1}$0) . (b) Corresponding temperature-dependent shift of the sample work function. The left inset depicts three exemplary PE spectra, the right shows the electron excitation scheme.

To gain insight into the atomic and electronic structure we employed DFT calculations. The use of semilocal approximations such as PBE is commonly criticized,[43,44] mainly because the corresponding Kohn-Sham orbital energies are usually not good approximations to ionization energies[61], because the self-interaction error[45] results in an underestimation of the binding energy of occupied orbitals and an overestimation of unoccupied orbitals. On the other hand, these functionals miss another important physical effect, namely the surface induced screening of the ionization energies after adsorption, also known as orbital renormalization.[47–50] Although both errors work in opposite directions, a fortuitous cancellation of errors should not be expected. We have thus carefully tested our approach by using hybrid functionals, which reduce the self-interaction error. This is reported in the appendix. In brief, we find that while PBE generally gives poor total work functions (that can be significantly improved using the HSE06 functional[53]), the work function *modification* or interface dipole is robust with respect to the choice of the functional. The stability of the results arises mainly from the fact that the lone pair orbital of pyridine and the valence band of ZnO, which are responsible for the binding to the surface, are almost equally affected by self-interaction.

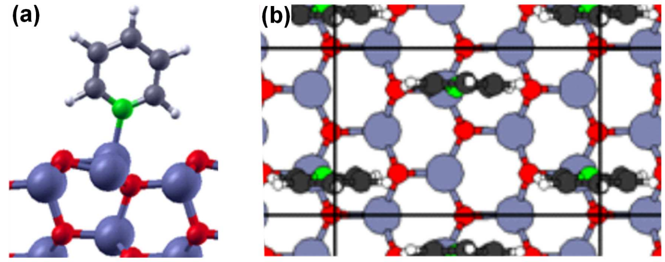

FIG. 2. (a): Side view of the PBE+vdW geometry of pyridine on ZnO(10$\bar{1}$0) (only a fraction of the unit cell is shown). (b) Top view of the unit cell of pyridine on ZnO(10$\bar{1}$0) at full coverage.

Having ascertained the reliability of our computational approach, we now turn to the characterization of the pyridine/ZnO(10$\bar{1}$0) interface. For a single molecule at low coverage we only find one stable geometry in contrast to metals, for which several different structures have been observed.[62] As shown in Figure 2, pyridine adsorbs upright with the nitrogen atom located directly above a surface Zn atom and the aromatic plane oriented along the (1120)-direction. Calculating the binding energy as

$$E_{Ads} = (E_{Sys} - E_{Mol} - E_{Slab}) \tag{2}$$

with E_{Sys} being the energy of the combined pyridine/ZnO system, E_{Mol} the energy of the free molecule in the gas phase and E_{Slab} the isolated ZnO(10$\bar{1}$0) surface, we find no other stable geometry with a binding energy larger than 0.1 eV/molecule. This finding is in excellent agreement with the one derived from the NEXAFS study of Walsh et al. for 0.1 ± 0.05 monolayer,[40] except for a slightly larger tilt angle (theory 15°, experiment 10°). Our calculations show that increasing the coverage (Θ) does not affect the tilt angle. The binding energy per unit area, calculated with equation 2 and divided by the area per molecule, is shown in Figure 3. A pronounced minimum is found at a layer density corresponding to 1 pyridine / 2 surface Zn atoms, which we will henceforth adopt as full monolayer coverage, $\Theta = 1.0$. The corresponding geometry is indicated in Figure 2. Further increasing the pyridine density will destabilize the layer, and the formation of a second layer which is not in direct contact with the substrate (shown in Figure 3 as open star) will be favored. Calculating different packing motifs for the second monolayer, we find several different minima exhibiting different dipole orientations to be within an energy range of 40 meV. Based on this theoretical information and the experimentally observed saturation of the work function near $\Theta = 1.0$, we speculate that the second layer grows amorphously and does not exhibit a net dipole moment.

Having determined the structure of the full monolayer, the adsorption-induced work function modifications were determined for a variety of coverages, down to 1/8 ML. In Figure 3b, the work function change in PBE+vdW is compared to the experimentally determined values. For the full monolayer coverage, a work function modification of -2.9 eV is obtained, in excellent agreement with the experimentally determined value. Also for lower Θ, remarkable agreement is found with a typical deviation of only $\approx$0.1 eV. However, it is noteworthy that around $\Theta = 0.75$, the curvature of the experimental and theoretical work function change does not agree well. We tentatively assign this to the fact that in the calculations a homogeneous removal of pyridine from the full monolayer was assumed, while in experiment the removal might occur irregularly or even patchwise. We re-emphasize, however, that all calculated points are within the experimental error ($\pm$ 0.05 ML). For $\Theta > 1$ (indicated by a dashed line in Figure 3), our calculations suggest that the work function remains constant if the additional pyridine is adsorbed forming an amorphous multilayer (see dashed line in Fig. 3). On the other hand, a further increase occurs if even more molecules could be forced into the first layer and be brought into direct contact with the substrate. As can be seen from the top panel of Fig. 3, only the first case is consistent with our total energy results and our PES/TDS measurements.

To determine whether the large interface dipole stems from the intrinsic molecular dipole or from charge-transfer to the substrate, we separate the total shift induced by the interface dipole $\Delta\Phi$, into a molecular part, $\Delta\Phi_{Mol}$, and an adsorption-induced shift, $\Delta\Phi_{Ads}$, using the equation

$$\Delta\Phi(\Theta) = \Delta\Phi_{Mol}(\Theta) + \Delta\Phi_{Ads}(\Theta) \tag{3}$$

Here, $\Delta\Phi$ was obtained from the calculation of the combined system as a function of coverage, while $\Delta\Phi_{Mol}$ was taken from a calculation of a hypothetical, free-standing pyridine layer in the same geometry of the adsorbed layer at the same density of molecules. Eq. 3 then becomes the definition of $\Delta\Phi_{Ads}$. Note that by this definition, $\Delta\Phi_{Ads}$ also contains the complete electronic response of the substrate upon adsorption, including the eventual formation of image dipoles. Since the geometry distortion of the surface upon adsorption induces only a minor dipole (<0.1 eV), we include this effect into $\Delta\Phi_{Ads}$, too. The results depicted in Figure 3 show that at low coverage the adsorption-induced dipole and the monolayer dipole act cooperatively and contribute roughly equally. Upon increasing the coverage, the dipoles depolarize. Comparing $\Delta\Phi_{Mol}$ with the hypothetical potential change in the absence of depolarization (calculated by inserting the dipole of the free molecule into eq. 1) shows that the dipole per molecule is reduced by $\approx$ 30% at full coverage. Up to

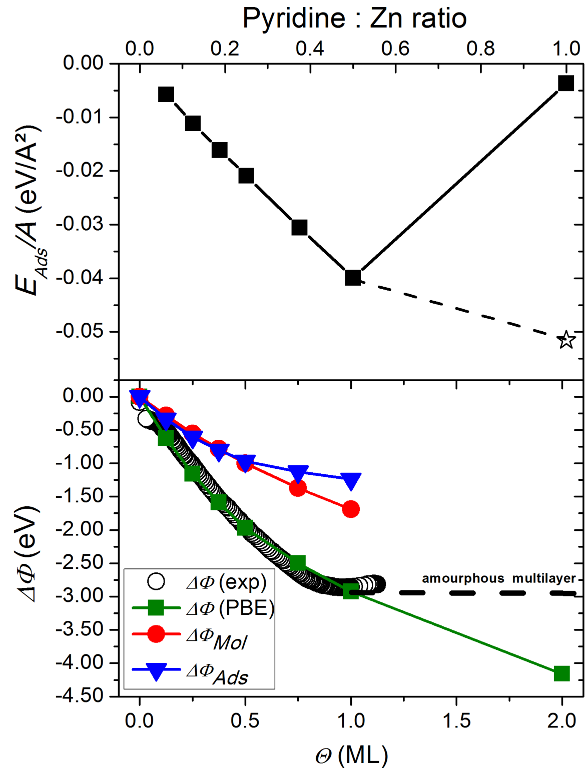

FIG. 3. Top: Calculated adsorption energy (PBE+vdW) per area as function of pyridine:Zn ratio. The dashed line and the open star denote the formation of an amorphous layer on top of the first pyridine layer. (b) Experimentally (open circles) and theoretically (closed squares) determined $\Delta\Phi$ as function of the pyridine coverage and its decomposition into its contributions E_{Ads} (triangles) and E_{Mol} (circles).

$\Theta = 0.5$, $\Delta\Phi_{Ads}$ shows the same evolution, illustrating that the pyridine-Zn bond is just as polarizable as the molecular dipole. For larger Θ, $\Delta\Phi_{Ads}$ decreases faster than $\Delta\Phi_{Mol}$ due to the increasing importance of repulsive through-substrate interactions.

More detailed insight into the bonding mechanism can be obtained by performing a molecular projected density of states (MODOS) analysis,[63] in which the density of states is decomposed into contributions from the individual molecular orbitals of the free monolayer. The result is shown in Figure 4a. We find that the PBE-HOMO is broadened considerably after adsorption, which reflects the very strong hybridization with the substrate bands and proves the formation of a covalent bond between ZnO($10\bar{1}0$) and pyridine. For comparison, the MODOS of the PBE-HOMO-1 is also shown. This orbital does not contribute to bonding and gives rise to a sharp peak. In this context, it is interesting to note that the self-interaction error of PBE leads to a reordering of the frontier orbitals of pyridine. Performing a MODOS analysis for HSE using larger values of α leads to a broadening of the lone-pair orbital in all cases, regardless of where it is located in the orbital hierarchy. Once again, this corroborates the conclusion that in the present system, electron self-interaction does not have a notable impact on the results. For each orbital, a formal electron occupation can be obtained by determining the fraction of its area below the Fermi-energy (the total area is normalized to 2 electrons). The results are shown in Figure 4b. Except for the PBE-HOMO, which contains 1.75 electrons after adsorption, no other orbital deviates significantly from its ideal occupation. Variation of the coverage unveils that the donation from the PBE-HOMO to ZnO always lies between 0.22 and 0.25 electrons and is thus practically independent of the pyridine density.

In semiconductors, the presence of charged species at the surface gives rise to band bending. Monitoring the d-band position and the electrostatic potential across a 32-layer slab for pyridine adsorption, we observed no band bending in our calculations, even when choosing doping concentrations that are so high that the extend of band bending is only a few Å. Thus, pyridine should not be viewed as a charged surface defect. Rather, the formal charge of pyridine reflects the polarity of the covalent pyridine-Zn bond, which gives rise to a potential that is screened out by the neighboring bonds already at intermolecular distances.[64] A more detailed discussion of the electrostatic potentials is given in the appendix.

One could now ask why such a large work function modification is possible with pyridine on ZnO($10\bar{1}0$) and, just as importantly, whether even larger reduction are conceivable and how they could be achieved. In principle the work function reduction upon adsorption is determined by the molecular dipole moment, the dipole moment induced by adsorption to the surface, and the packing density on the substrate. However, it has been demonstrated that the largest work function modification achievable with a given type of molecule is limited by its HOMO/LUMO, or, more precisely, by the HOMO/LUMO of the layer it forms.[65] The reason for this limitation is depicted in Figure 5. We assume a molecule with a dipole moment and an arbitrary positive electron affinity, as shown in Figure 5a. Forming a closed packed, free standing monolayer out of these molecule oriented such that the dipole point away from the surface will lead to a potential shift which brings the LUMO closer to the Fermi-energy of the substrate (Figure 5b). Upon contact with the surface, bonding can induce an additional potential that increases step until the LUMO comes into resonance with the Fermi energy. At this point, electrons start to be transferred from the substrate to the molecule, giving rise to a charge-transfer induced dipole moment pointing towards the surface. This effectively pins the EA to the Fermi energy (Figure 5c). The lower panel of Figure 5 depicts the same scenario, but now for a molecule with a LUMO above the vacuum level (i.e., a negative electron affinity) in both the gas phase (Figure 5d) and, after $\Delta\Phi_{Mol}$ is accounted for, also in the monolayer (Figure 5e). In this case, one can see that the vacuum level approaches the Fermi energy before the LUMO does. Of course, the vacuum level can never be below the Fermi energy in thermodynamic equilibrium without a constant external supply of electrons, meaning that the vacuum level eventually becomes pinned at E_F, yielding an effective work function for this system close to zero.

For pyridine, the negative EA in the gas phase fulfills our criterion, although with 0.6 eV the LUMO is close to the vacuum level. It would thus be conceivable that surface polarization induced renormalization of the molecular states (image effects) or polarizations in the molecular layer push the LUMO below the vacuum level. However, this seems not to be the case because for the full pyridine coverage our two-photon photoemission experiments do not show any unoccupied states between E_F and the vacuum level. We would thus expect that even larger work function reductions than the observed 2.9 eV should in principle be possible if the dipole density could be further increased.

Therefore, we now briefly discuss the hypothetical situation in which every Zn atom is bonded to a molecule. Although the aforementioned discussion demonstrates that this is not the most stable morphology under the experimental conditions described here, it might become stable at higher pyridine pressures. Figure 4 shows the MODOS for this coverage. The high packing density gives rise to stronger interactions between the pyridine molecule and thus to a stronger broadening of all molecular orbitals. The charge transfer from the HOMO is slightly reduced to 0.17e. However, even under these extreme conditions, the PBE-LUMO (which presents a lower limit for the true electron affinity) remains above the Fermi level and unoccupied. The additional molecules in the first layer further increase $\Delta\Phi$ to a total work function reduction of 4.2 eV, which translates into an effective pyridine/ZnO($10\bar{1}0$) -Φ of only 0.3 eV.

In general, many organic dyes, such as fluorene, rubrene, or porphyrine-derivates exhibit small electron affinities. For these, a strong work function reduction, as the one demonstrated here, will significantly lower the barrier for electron injection. At the same time, the transport of holes cannot occur through the pyridine HOMO, which is strongly hybridized and exhibits only little density of states in the ZnO gap. Pyridine on ZnO($10\bar{1}0$) is therefore also expected to improve the hole-blocking properties of this interface. The level alignment is thus particularly beneficial for light-emitting diodes, where it is expected to increase the residual time of charge carriers in the active organic material. Of course, the low thermal stability of this particular interface must be considered as a significant drawback for the use in actual devices. However, we are confident that this can be overcome by suitable chemical modifications of pyridine or other molecules that fulfill the same electronic requirements.

IV. CONCLUSION

The adsorption of pyridine on ZnO($10\bar{1}0$) was studied using thermal desorption and photoelectron spectroscopy as well as density functional theory. Experiment and theory concurrently show that pyridine substantially reduces the work function by up to 2.9 eV. Pyridine is found to adsorb upright-standing with all pyridine molecules aligned parallel to each other. In a closed monolayer, the organic material is bonded to every second surface Zn atom. Our investigation reveals that this large work function change is due to a cooperative effect between the intrinsic molecular and the adsorption-induced dipole, in particular the formation of a strongly polar bond between pyridine and surface Zn atoms. The large work-function change is made possible by the fact that the electron affinity of the layer remains above the vacuum level, which prevents the occurrence of Fermi-level pinning.

To validate the theoretical findings, hybrid functionals with a variable fraction of exact exchange, α, have been applied. We see that the Kohn-Sham eigenvalues do not agree well with the experimental ionization energies, and, moreover, tuning α as single free parameter is not sufficient to achieve a quantitatively correct level alignment between substrate and organic material. Nonetheless, the observable of interest, the work function modification (but not the work function itself) is well reproduced independent of the functional used.

ACKNOWLEDGMENTS

We thank A. Tkatchenko and G.-X. Zhang for supplying the van-der-Waals parameters, E. Zojer, D.A. Egger, B. Bieniek, and N. Moll for fruitful discussions, and funding by the Deutsche Forschungsgemeinschaft through SFB 951 and by the Austrian Science Fund FWF through the Erwin-Schrödinger grant J 3258-N20. Y. Xu acknowledges support by the Alexander von Humboldt foundation.

V. APPENDIX A: FUNCTIONAL TESTS

Semilocal density functional theory, the most popular method in theoretical interface science, suffers from the so-called self-interaction error (SIE), i.e., the interaction of electrons with themselves.[45] Additionally, the band-gap renormalization after adsorption on the surface or the screening of charge due to the surrounding organic molecules is not captured in the orbital energies.[47–50] All this worsens the description of the relative level alignment. In pathological cases, this might lead to qualitatively wrong interactions[66–68] or even adsorption geometries.[69,70] Typically, adsorbate and substrate are affected differently and no fortuitous error cancellation should be expected. In pathological cases, the relative level ordering could even be qualitatively wrong, which may lead to spurious charge transfer.[68] Straightforward theoretical solutions exist, e.g., the self-consistent GW approach[71,72] or the random phase approximation,[73–77] which can be further extended using single excitations[78] and second-order screened exchange.[79,80] Unfortunately, these functionals are computationally very expensive and not yet tractable for the unit cells of realistic inorganic/organic interfaces, which typically contain more than 100 atoms. An alternative solution is to use hybrid functionals. They add a fraction of exact exchange, α, to semilocal functionals in order to mitigate the self-interaction error, although this does not cure the missing band-gap renormalization.[50] Hybrid functionals have already been successfully applied to studies of defects in solids,[81–86] where a considerable impact of α on the relative position of defect level and host band-edges as well as on defect formation energies have been discussed. Although hybrid functional studies for molecules on clusters are comparatively abundant, calculations for extended inorganic/organic interfaces (which can differ significantly from the cluster case[87,88]) are only just emerging.[50,89]

In hybrid functionals, a fraction α of semilocal exchange (in the case of PBE (E_x^{PBE})) is replaced by exact exchange (E_x^{exact}), while correlation is retained fully at the semilocal level (E_c^{PBE}).

$$E_{xc} = \alpha E_x^{exact} + (1-\alpha)E_x^{PBE} + E_c^{PBE} \tag{4}$$

In addition, the exchange-correlation energy can be separated into a short-range and a long-range contribution. The separation is controlled by the parameter ω. In HSE, the exact-exchange contribution is short-ranged, while the long range is treated by a standard semilocal approach. Physically, ω is often interpreted as an electronic screening length.[53] In the present contribution, we studied the impact of hybrid functionals by varying α, while keeping ω at its suggested values of 0.2Å^{-1}.[53] One of the disadvantages of hybrid functionals is the absence of rigorous criteria for the choice of α, which in principle should be a material-dependent parameter.[90] This is an obvious problem for adsorption calculations, where potentially two very different α would be needed to correctly describe substrate and adsorbate. It has been proposed to make α dependent on the local electron density,[91] but the functional dependence is not known. For a first principles approach, we therefore prefer to employ a single parameter for the whole system.

For the systems considered here, the band-gap problem is summarized in Figure 6. Panel (a) shows the position of the valence band maximum (VBM) and conduction band minimum (CBM) of ZnO($10\bar{1}0$) relative to the vacuum level above the unreconstructed surface as function of α using the geometry obtained with PBE+vdW. At $\alpha = 0$ (i.e., for PBE), we obtain a band gap of only 0.92 eV, in agreement with previous reports.[96,97] The absolute values of the VBM and CBM are equally unsatisfactory and are found significantly above and below the experimental results. Upon increasing α, both values get closer to experiment and eventually overshoot. The impact of exact exchange is stronger for the VBM than the CBM, due to their different character (s vs. p). A reasonably quantitative agreement between theory and experiment is obtained for $\alpha \approx 0.4$, which is close to the value of 0.375 suggested by Oba et al.[96] Some of us have recently established a correlation between defect formation energies and the valence band width as a measure of the cohesive energy.[82] For ZnO, the HSE valence bandwidth best agrees with experiment at $\alpha \approx 0.6$ (Figure 6c). Also the experimental position of the d-band, which is 7.5 eV below the VBM, is best reproduced for this value of α.

In panel b, an equivalent study for the isolated pyridine molecule in the gas phase is presented. We chose the isolated molecule and not a pyridine monolayer, because experimental spectroscopic data is available. However, it should be kept in mind that the properties of an extended (sub)monolayer are distinctively different,[13] due to collective effects such as (de)polarization of dipoles,[64,87] screening effects[98,99] and other electrostatic effects.[88] Even thin molecular layers behave like crystals, implying that their ionization energies are strongly dependent on their orientation and morphology.[100] For pyridine, the strong impact is illustrated by contrasting the work of Han et al., who found a negative electron affinity for extended pyridine clusters,[101] with measurements of Otto et al., who determined the electron affinity for ordered pyridine layers of Ag(111) to be positive.[32] To not bias our results by assuming a given morphology, we decided to study the impact of exact exchange on pyridine for the isolated molecule in the gas phase.

For DFT calculations, pyridine is a particular pathological molecule suffering strongly from self-interaction. In the gas phase, this small conjugated organic molecule exhibits a vertical ionization potential of 9.6 eV.[102] Its electron affinity is negative, i.e. its lowest unoccupied molecular orbital is located 0.62 eV above the vacuum level,[32,94,103] giving rise to a fundamental gap in excess of 10 eV. In exact density functional theory, the HOMO should equal the ionization potential.[104] For no other state such an exact relation exists. In analogy to the work of Kronik et al.,[90] we make use of the fact that the ionization potential of the negatively charged molecule is, by definition, equal to the electron affinity of the neutral molecule. Therefore, to determine the "best" α, we compare the DFT-HOMO of the neutral molecule with the ionization potential and the singly occupied molecular orbital (DFT-SOMO) of the radical anion with the electron affinity. For α=0, we find a DFT-HOMO energy of -5.9 eV and a DFT-SOMO energy of -1.9 eV. However, even when increasing α all the way to 1, the experimental ionization energies are never reproduced and their energies are underestimated. This is because HSE is a short-range hybrid functional and its potential therefore exhibits the wrong asymptotic decay. On the other hand, taking the total energy difference between the charged and the neutral molecules (called ΔSCF-approach), yields results in good agreement with experiment, irrespective of the fraction of exact exchange. Another peculiarity that can be observed in Figure 6b is that the slope of the DFT-HOMO as a function of α changes around $\alpha \approx 0.2$. The reason for this is a reordering of the occupied orbitals. PBE incorrectly predicts the nitrogen lone pair as the DFT-HOMO.[105] Exact exchange affects the localized lone-pair more strongly than the π-orbitals, and thus this orbital, which will be responsible for the binding to the substrate, becomes the DFT-HOMO-1 for $0.2 < \alpha < 0.8$ and the DFT-HOMO-2 for $\alpha > 0.8$. Despite these changes, the electron density difference upon ionization (in analogy to the ΔSCF-approach calculated as the difference between the electron density of the positively charged and the neutral molecule) is qualitatively the same at all α, being reminiscent of the lone pair orbital.

Although the strong dependence of the levels on α is unsettling, we reiterate that Kohn-Sham levels are not physical observables *per se*, and that even the DFT-HOMO-energy should be expected to be different from the IP when using a functional with an incorrect asymptotic behavior. We therefore instead assess the quality of our calculations based on the observable of interest for the combined system, the interface dipole $\Delta\Phi$. The impact of α, as shown in Figure 6d, is acceptably small, differing less than 10% between α=0.0 and α=1.0. We attribute this stability of the results to the fact that, on the one hand, the lone pair orbital of pyridine (which is responsible for binding), shifts almost parallel with the valence band onset of ZnO when increasing α. On the other hand, a change of α in this system never leads to a crossing of pyridine orbitals with the Fermi-energy and thus a qualitatively incorrect ordering of orbitals. Note that this variation is significantly smaller than that reported for, e.g., aminobiphenyl on gold clusters.[43]

VI. APPENDIX B: ELECTROSTATIC POTENTIALS

More detailed insight into the mechanism behind the work-function change and the reason for the absence of band bending can be obtained by inspecting the change in the electrostatic potential induced by a monolayer of pyridine. The evolution of the electrostatic potential is known to depend qualitatively on the dimensionality and packing density of the adsorbate.[64,88] For 2D-periodic systems, Natan et al. used electrostatic arguments to show that the field decays to 1/e at a distance of $\frac{d}{2\pi}$, where d is the distance between the organic molecules.[64] For a full monolayer of pyridine, the distance between adjacent molecules is 6.3 Å. This leads to a natural decay length of approx. 1.0 Å, which is significantly shorter than the Zn-N bond (2.12 Å). For a hypothetical, free-standing monolayer of pyridine in the same geometry as the full monolayer, the evolution of the plane-averaged total potential, including also exchange and correlation contributions, is shown in the left panel of Figure 7. The Figure clearly shows that at the position of the topmost Zn atom, the electron potential energy has already almost converged to the vacuum level (with a deviation of only 7 meV). Note that the difference between the converged potential energy on the left and the right side of the monolayer corresponds to the potential shift induced the by monolayer, designated $\Delta\Phi_{Mol}$ in the main text. It would now be natural to ask how quickly the electron potential originating for the adsorption-induced electron rearrangements decays. To answer this question, we solved the Poisson-equation for the adsorption induced electron rearrangements, $\Delta\rho$, which was calculated as

$$\Delta\rho = \rho^{sys} - \rho^{slab} - \rho^{monolayer} \tag{5}$$

where ρ^{sys} is the electron density of the combined system, ρ^{slab} of the ZnO slab, and $\rho^{monolayer}$ of the free-standing pyridine monolayer. The plane-averaged result is shown in the right panel of Figure 7. Similar to the molecular component, the averaged electron potential quickly converges to a constant level. Within the slab, the second ZnO double layer (at approx. -5 Å relative to the nitrogen atom) is less than 1 meV away from the converged value at the left hand side.

VII. REFERENCES

[1] T. K. Gupta, Journal of the American Ceramic Society **73**, 1817 (1990).
[2] B. D. Huey, D. Lisjak, and D. A. Bonnell, Journal of the American Ceramic Society **82**, 1941 (1999).
[3] S. Hirose, K. Nishita, and H. Niimi, Journal of Applied Physics **100**, 083706 (2006).
[4] J. S. Kim, M. Granstrom, R. H. Friend, N. Johansson, W. R. Salaneck, R. Daik, W. J. Feast, and F. Cacialli, Journal of Applied Physics **84**, 6859 (1998).
[5] J. Robertson, Journal of Vacuum Science Technology B: Microelectronics and Nanometer Structures **18**, 1785 (2000).
[6] G. Ashkenasy, D. Cahen, R. Cohen, A. Shanzer, and A. Vilan, Accounts of Chemical Research **35**, 121 (2002).
[7] N. Koch, ChemPhysChem **8**, 1438 (2007).
[8] H. Ishii, K. Sugiyama, D. Yoshimura, E. Ito, Y. Ouchi, and K. Seki, IEEE Journal of Selected Topics in Quantum Electronics **4**, 24 (1998).
[9] I. G. Hill, A. Rajagopal, A. Kahn, and Y. Hu, Applied Physics Letters **73**, 662 (1998).
[10] F. Nuesch, F. Rotzinger, L. Si-Ahmed, and L. Zuppiroli, Chemical Physics Letters **288**, 861 (1998).
[11] J. Blochwitz, T. Fritz, M. Pfeiffer, K. Leo, D. Alloway, P. Lee, and N. Armstrong, Organic Electronics **2**, 97 (2001).
[12] X. Crispin, V. Geskin, A. Crispin, J. Cornil, R. Lazzaroni, W. R. Salaneck, and J.-L. Bredas, Journal of the American Chemical Society **124**, 8131 (2002).
[13] H. Ishii, K. Sugiyama, E. Ito, and K. Seki, Advanced Materials **11**, 605 (1999).
[14] I. H. Campbell, S. Rubin, T. A. Zawodzinski, J. D. Kress, R. L. Martin, D. L. Smith, N. N. Barashkov, and J. P. Ferraris, Physical Review B **54**, 14321 (1996).
[15] C. Boulas, J. Davidovits, F. Rondelez, and D. Vuillaume, Physical Review Letters **76**, 4797 (1996).
[16] I. H. Campbell, J. D. Kress, R. L. Martin, D. L. Smith, N. N. Barashkov, and J. P. Ferraris, Applied Physics Letters **71**, 3528 (1997).
[17] R. W. Zehner, B. F. Parsons, R. P. Hsung, and L. R. Sita, Langmuir **15**, 1121 (1999).
[18] L. Zuppiroli, L. Si-Ahmed, K. Kamaras, F. Nuesch, M. N. Bussac, D. Ades, A. Siove, E. Moons, and M. Gratzel, The European Physical Journal B **11**, 505 (1999).
[19] C. Ganzorig, K.-J. Kwak, K. Yagi, and M. Fujihira, Applied Physics Letters **79**, 272 (2001).
[20] R. Hatton, Thin Solid Films **394**, 291 (2001).
[21] P. Hartig, T. Dittrich, and J. Rappich, Journal of Electroanalytical Chemistry **524-525**, 120 (2002).
[22] H. Yan, Q. Huang, J. Cui, J. Veinot, M. Kern, and T. Marks, Advanced Materials **15**, 835 (2003).
[23] D. Alloway, M. Hofmann, D. Smith, N. Gruhn, A. Graham, R. Colorado Jr, V. Wysocki, T. Lee, P. Lee, and N. Armstrong, The Journal of Physical Chemistry B **107**, 11690 (2003).
[24] G. Heimel, L. Romaner, E. Zojer, and J.-L. Bredas, Nano Letters **7**, 932 (2007).
[25] B. de Boer, A. Hadipour, M. M. Mandoc, T. van Woudenbergh, and P. W. M. Blom, Advanced Materials **17**, 621 (2005).
[26] L. Lindell, M. Unge, W. Osikowicz, S. Stafstrom, W. R. Salaneck, X. Crispin, and M. P. de Jong, Applied Physics Letters **92**, 163302 (2008).
[27] J.-G. Wang, E. Prodan, R. Car, and A. Selloni, Physical Review B **77**, 245443 (2008).
[28] G. Latini, M. Wykes, R. Schlapak, S. Howorka, and F. Cacialli, Applied Physics Letters **92**, 013511 (2008).
[29] I. Csik, S. P. Russo, and P. Mulvaney, The Journal of Physical Chemistry C **112**, 20413 (2008).
[30] Y. Zhou, C. Fuentes-Hernandez, J. Shim, J. Meyer, A. J. Giordano, H. Li, P. Winget, T. Papadopoulos, H. Cheun, J. Kim, M. Fenoll, A. Dindar, W. Haske, E. Najafabadi, T. M. Khan, H. Sojoudi, S. Barlow, S. Graham, J.-L. Bredas, S. R. Marder, A. Kahn, and B. Kippelen, Science **336**, 327 (2012).
[31] J. Gland and G. Somorjai, Surface Science **38**, 157 (1973).
[32] A. Otto, K. Frank, and B. Reihl, Surface Science **163**, 140 (1985).
[33] G. Eesley, Physics Letters A **81**, 193 (1981).
[34] D. Heskett, L. Urbach, K. Song, E. Plummer, and H. Dai, Surface Science **197**, 225 (1988).
[35] F. P. Netzer, G. Rangelov, G. Rosina, and H. B. Saalfeld, The Journal of Chemical Physics **89**, 3331 (1988).
[36] J. Whitten, Surface Science **546**, 107 (2003).
[37] Z. Ma, F. Rissner, L. Wang, G. Heimel, Q. Li, Z. Shuai, and E. Zojer, Physical Chemistry Chemical Physics **13**, 9747 (2011).
[38] C. Wang, A. S. Batsanov, M. R. Bryce, S. Martin, R. J. Nichols, S. J. Higgins, V. M. M. Garcia-Suarez, and C. J. Lambert, Journal of the American Chemical Society **131**, 15647 (2009).
[39] C. Woll, Progress in Surface Science **82**, 55 (2007).
[40] J. Walsh, R. Davis, C. Muryn, G. Thornton, V. Dhanak, and K. Prince, Physical Review B **48**, 14749 (1993).
[41] S. Hovel, C. Kolczewski, M. Wuhn, J. Albers, K. Weiss, V. Staemmler, and C. Woll, The Journal of Chemical Physics **112**, 3909 (2000).
[42] A. Tkatchenko and M. Scheffler, Physical Review Letters **102**, 073005 (2009).
[43] E. Fabiano, M. Piacenza, S. D'Agostino, and F. Della Sala, The Journal of Chemical Physics **131**, 234101 (2009).
[44] J. Martinez, E. Abad, C. Gonzlez, J. Ortega, and F. Flores, Organic Electronics **13**, 399 (2012).
[45] J. P. Perdew, Physical Review B **23**, 5048 (1981).

[46] P. Mori-Sanchez, A. J. Cohen, and W. Yang, The Journal of Chemical Physics **125**, 201102 (2006).
[47] J. Neaton, M. Hybertsen, and S. Louie, Physical Review Letters **97**, 216405 (2006).
[48] J. M. Garcia-Lastra, C. Rostgaard, A. Rubio, and K. S. Thygesen, Physical Review B **80**, 245427 (2009).
[49] K. Thygesen and A. Rubio, Physical Review Letters **102**, 046802 (2009).
[50] A. Biller, I. Tamblyn, J. B. Neaton, and L. Kronik, The Journal of Chemical Physics **135**, 164706 (2011).
[51] V. Blum, R. Gehrke, F. Hanke, P. Havu, V. Havu, X. Ren, K. Reuter, and M. Scheffler, Computer Physics Communications **180**, 2175 (2009).
[52] J. P. Perdew, K. Burke, and M. Ernzerhof, Physical Review Letters **77**, 3865 (1996).
[53] A. V. Krukau, O. A. Vydrov, A. F. Izmaylov, and G. E. Scuseria, The Journal of Chemical Physics **125**, 224106 (2006).
[54] G.-X. Zhang, A. Tkatchenko, J. Paier, H. Appel, and M. Scheffler, Physical Review Letters **107**, 245501 (2011).
[55] A. Janotti and C. G. Van de Walle, Reports on Progress in Physics **72**, 126501 (2009).
[56] M. Scheffler, Physica B+C **146**, 176 (1987).
[57] N. A. Richter, S. Sicolo, S. V. Levchenko, J. Sauer, and M. Scheffler, Physical Review Letters **111**, 045502 (2013).
[58] N. Moll, Y. Xu, O. T. Hofmann, and P. Rinke, New. J.Phys. **15**, 083009 (2013).
[59] Y. Xu, O. T. Hofmann, R. Schlesinger, S. Winkler, J. Frisch, J. Niederhausen, A. Vollmer, S. Blumstengel, F. Henneberger, N. Koch, P. Rinke, and M. Scheffler, available online: http://arxiv.org/abs/1306.4580.
[60] Q. Zhong, C. Gahl, and M. Wolf, Surface Science **496**, 21 (2002).
[61] The words HOMO and LUMO are commonly used to denote the electronic levels associated with the experimental ionization potential and electron affinity. In order to avoid confusion, we use the prefixes "PBE-" or "DFT-" for levels obtained by density functional theory.
[62] F. P. Netzer and M. G. Ramsey, Critical Reviews in Solid State and Materials Sciences **17**, 397 (1992).
[63] C. J. Nelin, P. S. Bagus, and M. R. Philpott, The Journal of Chemical Physics **87**, 2170 (1987).
[64] A. Natan, L. Kronik, H. Haick, and R. Tung, Advanced Materials **19**, 4103 (2007).
[65] D. A. Egger, F. Rissner, G. M. Rangger, O. T. Hofmann, L. Wittwer, G. Heimel, and E. Zojer, Physical Chemistry Chemical Physics **12**, 4291 (2010).
[66] J. P. Perdew, A. Ruzsinszky, L. A. Constantin, J. Sun, and G. I. Csonka, Journal of Chemical Theory and Computation **5**, 902 (2009).
[67] A. Ruzsinszky, J. P. Perdew, G. I. Csonka, O. A. Vydrov, and G. E. Scuseria, The Journal of Chemical Physics **125**, 194112 (2006).
[68] I. Avilov, V. Geskin, and J. Cornil, Advanced Functional Materials **19**, 624 (2009).
[69] P. J. Feibelman, B. Hammer, J. K. Norrskov, F. Wagner, M. Scheffler, R. Stumpf, R. Watwe, and J. Dumesic, The Journal of Physical Chemistry B **105**, 4018 (2001).
[70] X. Ren, P. Rinke, and M. Scheffler, Physical Review B **80**, 045402 (2009).
[71] F. Caruso, P. Rinke, X. Ren, M. Scheffler, and A. Rubio, Physical Review B **86**, 081102 (2012).
[72] F. Caruso, P. Rinke, X. Ren, A. Rubio, and M. Scheffler, Phys. Rev. B **88**, 075105 (2013).
[73] D. Langreth and J. Perdew, Physical Review B **21**, 5469 (1980).
[74] J. Perdew, Physical Review B **33**, 8822 (1986).
[75] Z. Yan, J. Perdew, and S. Kurth, Physical Review B **61**, 16430 (2000).
[76] M. Rohlfing and T. Bredow, Physical Review Letters **101**, 266106 (2008).
[77] X. Ren, P. Rinke, C. Joas, and M. Scheffler, J. Mater. Sci. **47**, 21 (2012).
[78] X. Ren, A. Tkatchenko, P. Rinke, and M. Scheffler, Phys. Rev. Lett. **106**, 153003 (2011).
[79] A. Gruneis, M. Marsman, J. Harl, L. Schimka, and G. Kresse, The Journal of Chemical Physics **131**, 154115 (2009).
[80] J. Paier, X. Ren, P. Rinke, G. E. Scuseria, A. Gruneis, G. Kresse, and M. Scheffler, New Journal of Physics **14**, 043002 (2012).
[81] A. Janotti, J. B. Varley, P. Rinke, N. Umezawa, G. Kresse, and C. G. Van de Walle, Physical Review B **81**, 085212 (2010).
[82] R. Ramprasad, H. Zhu, P. Rinke, and M. Scheffler, Physical Review Letters **108**, 066404 (2012).
[83] A. Alkauskas, P. Broqvist, and A. Pasquarello, physica status solidi (b) **248**, 775 (2011).
[84] H.-P. Komsa, P. Broqvist, and A. Pasquarello, Physical Review B **81**, 205118 (2010).
[85] P. Rinke, A. Janotti, M. Scheffler, and C. Van de Walle, Physical Review Letters **102**, 026402 (2009).
[86] H. Li, L. K. Schirra, J. Shim, H. Cheun, B. Kippelen, O. L. A. Monti, and J.-L. Bredas, Chemistry of Materials **24**, 3044 (2012).
[87] D. Deutsch, A. Natan, Y. Shapira, and L. Kronik, Journal of the American Chemical Society **129**, 2989 (2007).
[88] F. Rissner, A. Natan, D. A. Egger, O. T. Hofmann, L. Kronik, and E. Zojer, Organic Electronics **13**, 3165 (2012).
[89] N. Sai, K. Leung, and J. Chelikowsky, Physical Review B **83**, 121309 (2011).
[90] L. Kronik, T. Stein, S. Refaely-Abramson, and R. Baer, Journal of Chemical Theory and Computation **8**, 1515 (2012).
[91] J. Jaramillo, G. E. Scuseria, and M. Ernzerhof, The Journal of Chemical Physics **118**, 1068 (2003).
[92] K. Jacobi, G. Zwicker, and A. Gutmann, Surface Science **141**, 109 (1984).
[93] S. Lias, *NIST Chemistry Webbook, NIST standard reference Database Number 69: "Pyridine - Gas phase ion energetics data"*, edited by S. Lias (National Institute of Standards and Technology, 2013).
[94] I. Nenner, The Journal of Chemical Physics **62**, 1747 (1975).
[95] R. Powell, W. Spicer, and J. McMenamin, Physical Review B **6**, 3056 (1972).
[96] F. Oba, A. Togo, and I. Tanaka, Physical Review B **77** (2008).
[97] A. Janotti and C. G. Van de Walle, physica status solidi (b) **248**, 799 (2011).
[98] E. F. Valeev, V. Coropceanu, D. A. da Silva Filho, S. Salman, and J.-L. Bredas, Journal of the American Chemical Society **128**, 9882 (2006).
[99] S. Sharifzadeh, A. Biller, L. Kronik, and J. Neaton, Physical Review B **85** (2012).
[100] S. Duhm, G. Heimel, I. Salzmann, H. Glowatzki, R. L. Johnson, A. Vollmer, J. P. Rabe, and N. Koch, Nature Materials **7**, 326 (2008).
[101] S. Y. Han, J. K. Song, J. H. Kim, H. B. Oh, and S. K. Kim, The Journal of Chemical Physics **111**, 4041 (1999).
[102] J. Eland, J. Berkowitz, H. Schulte, and R. Frey, International Journal of Mass Spectrometry and Ion Physics **28**, 297 (1978).
[103] K.-H. Frank, R. Dudde, and E. Koch, Chemical Physics Letters **132**, 83 (1986).
[104] J. Janak, Physical Review B **18**, 7165 (1978).
[105] N. Marom, F. Caruso, X. Ren, O. T. Hofmann, T. Korzdorfer, J. Chelikowsky, A. Rubio, M. Scheffler, and P. Rinke, Physical Review B **86**, 245127 (2012).

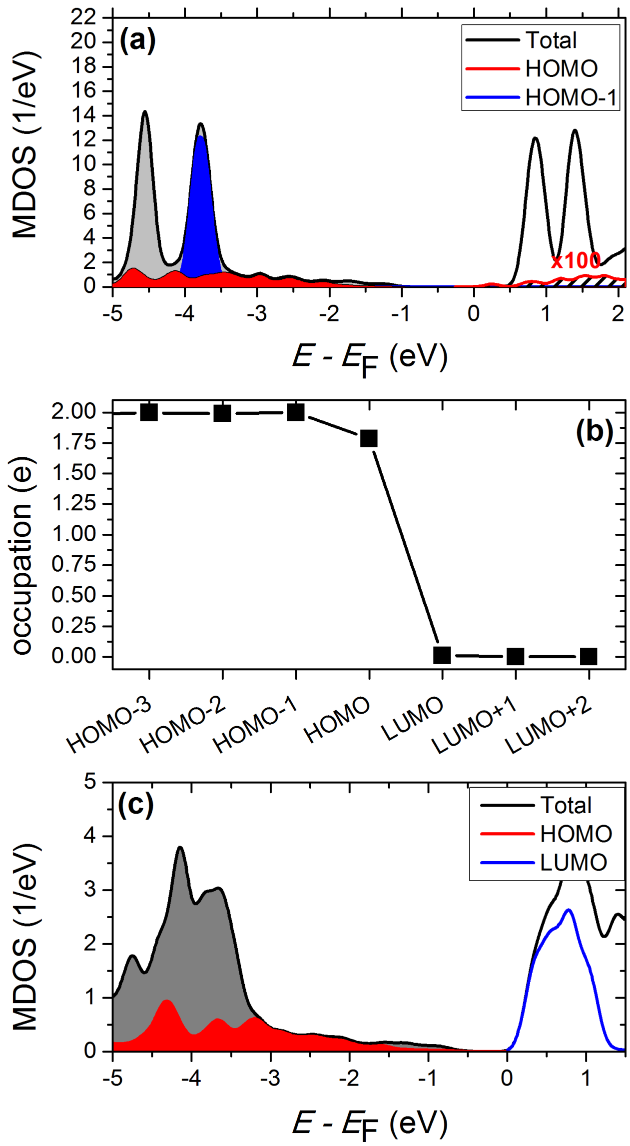

FIG. 4. (a): Molecular orbital projected density of states for pyridine at a pyridine/Zn ratio of 1:2 (one monolayer). The total projection onto pyridine is shown in black, the contribution of the PBE-HOMO is shown in red, and the contribution of the PBE-HOMO-1 is shown in blue. Filled areas are occupied. For the sake of clarity, the contribution of the former PBE-HOMO that lies above the Fermi energy and is now unoccupied is magnified by a factor of 100 and indicated by shading. (b) Formal occupation of the molecular orbtials, obtained by integration of the MODOS up to E_F. (c) Molecular orbtial projected density of states for pyridine at a pyridine/Zn ration of 1:1. The total projection of pyridine is shown in black, the contribution of the HOMO in red, the contribution of the PBE-LUMO in blue. Shaded areas are occupied.

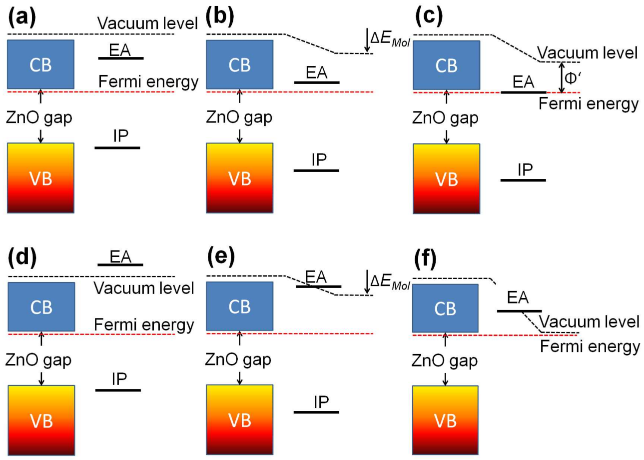

FIG. 5. Fermi-level pinning for systems with positive EA (top) and negative EA (bottom). See main text for detailed explanation.

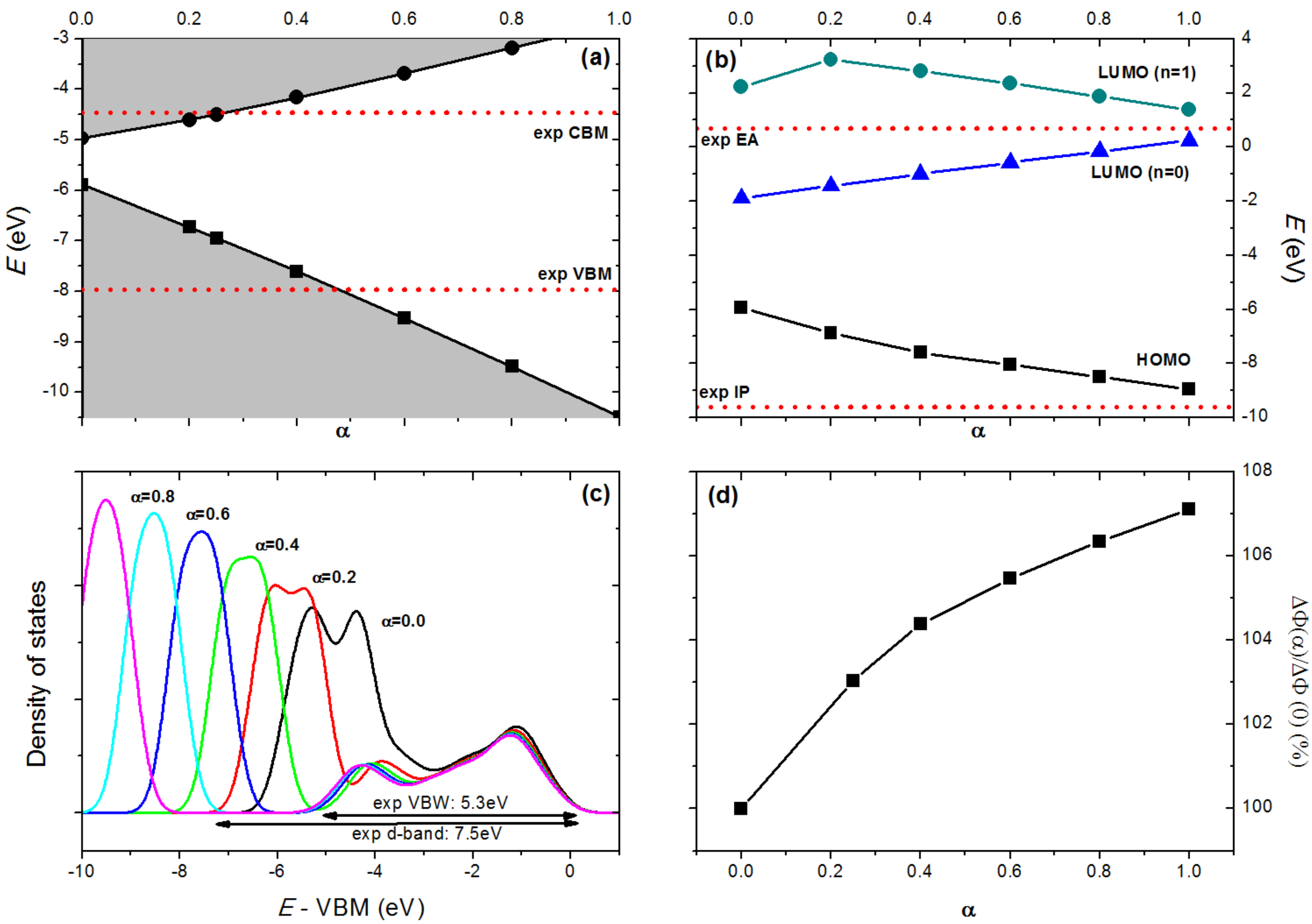

FIG. 6. (a): Valence and conduction band onsets in HSE for ZnO($10\bar{1}0$) (black lines) vs. experimental results (red dashes).[92] (b) Eigenvalues of the pyridine DFT-HOMO (black sqaures), empty DFT-LUMO (cyano circles) and DFT-SOMO of the radical anion (red triangles) vs experimental IP[93] and EA[94] (red dashes). (c) Density of states for ZnO, broadenend by 0.3 eV, compared to the experimental values for the valence band width (VBW)[95] and *d*-band position.[95] (d) Change of the interface dipole relative to the PBE -value as functional of the parameter α for a full monolayer of pyridine on ZnO($10\bar{1}0$)

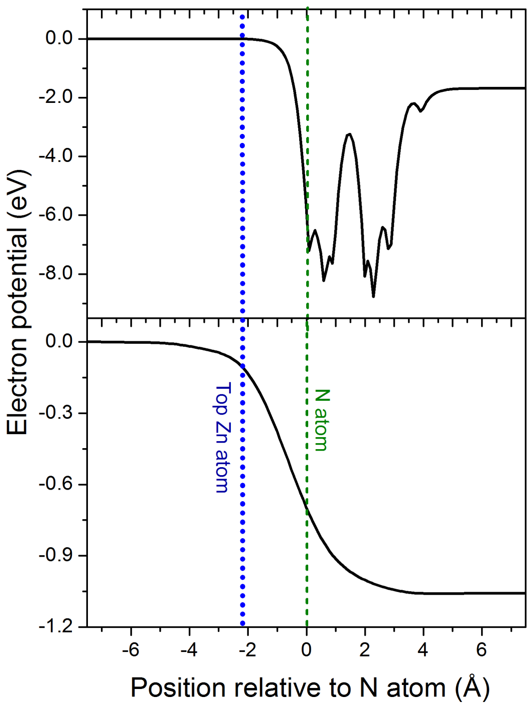

FIG. 7. Left: Electron potential energy for a hypothetical, free-standing pyridine monolayer in PBE. Right: Electron potential energy originating from the charge-rearrangements upon adsorption of a full monolayer of pyridine on ZnO($10\bar{1}0$) (bond dipole) as obtained by PBE.